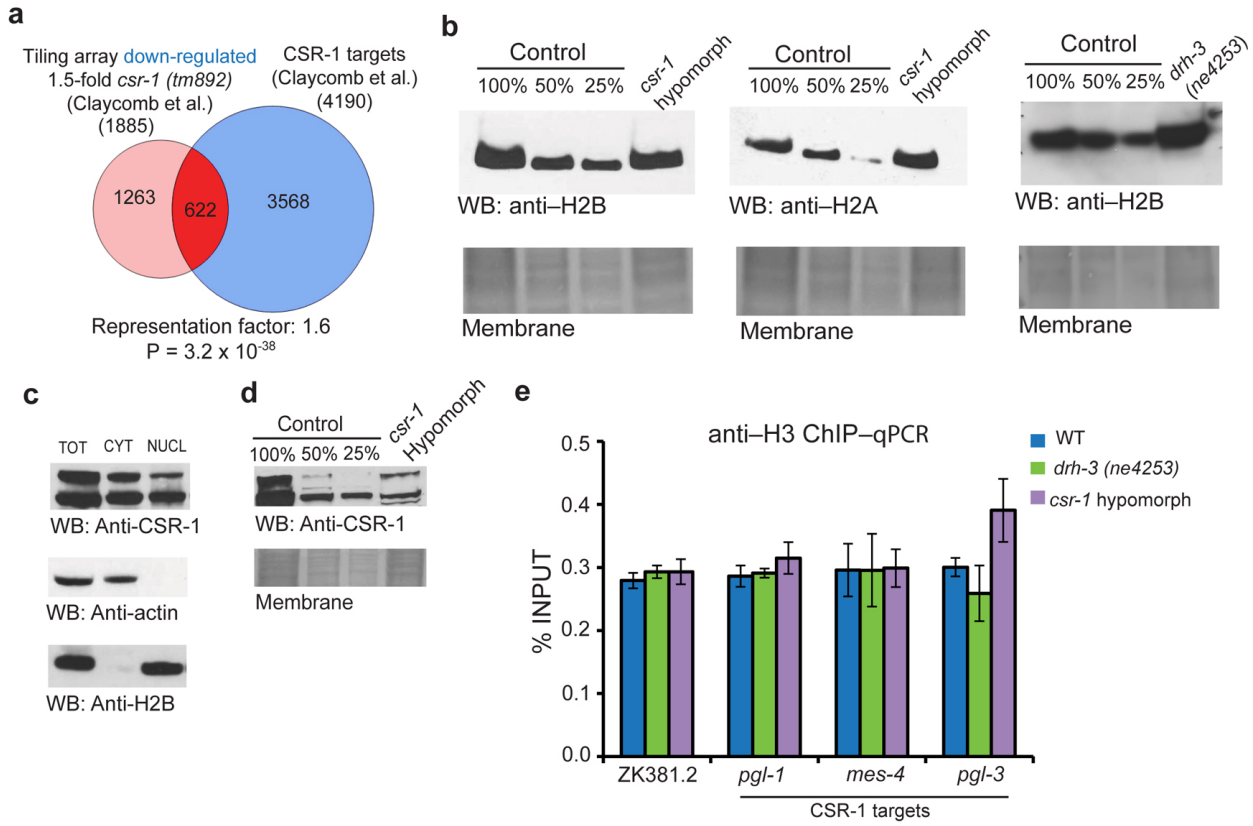

Supplementary Figure 1. Histone abundance is not compromised in *csr-1* hypomorph and *drh-3(ne4253)* mutant worms. (a) Venn diagram showing an overlap between genes down-regulated at least 1.5 fold in *csr-1(tm892)* mutant (by tiling array[15]) and CSR-1 target genes[15]. A Fisher's exact test was used for calculating a P value for the significance of the overlap. **(b)** Western blotting showing that the levels of H2B (left panel) and H2A (center panel) in *csr-1* hypomorph and the level of H2B in *drh-3(ne4253)* mutant (right panel) are not reduced compared to the control. Ponceau red staining is shown as a loading control (membrane). **(c)** Western blot showing the two isoforms of CSR-1 present in the cytoplasmic and nuclear fractions (top panel). In control western blots histone H3 is detected in the nuclear fraction (bottom panel) and actin is detected in the cytoplasmic fraction (middle panel). **(d)** Western blot showing reduced levels of CSR-1 in nuclear extracts from *csr-1* hypomorph compared to the control. Ponceau red staining is shown as a loading control (membrane). **(e)** ChIP-qPCR results with histone H3 antibody detect no significant changes in the incorporation of histone proteins into chromatin at selected germline-specific CSR-1 targets and non-target loci in *csr-1* hypomorph and *drh-3 (ne4253)* mutants in comparison to WT. Data are presented as the mean of the percentage of input in three independent experiments. Error bars, s.d. (n = 3 nematode cultures).

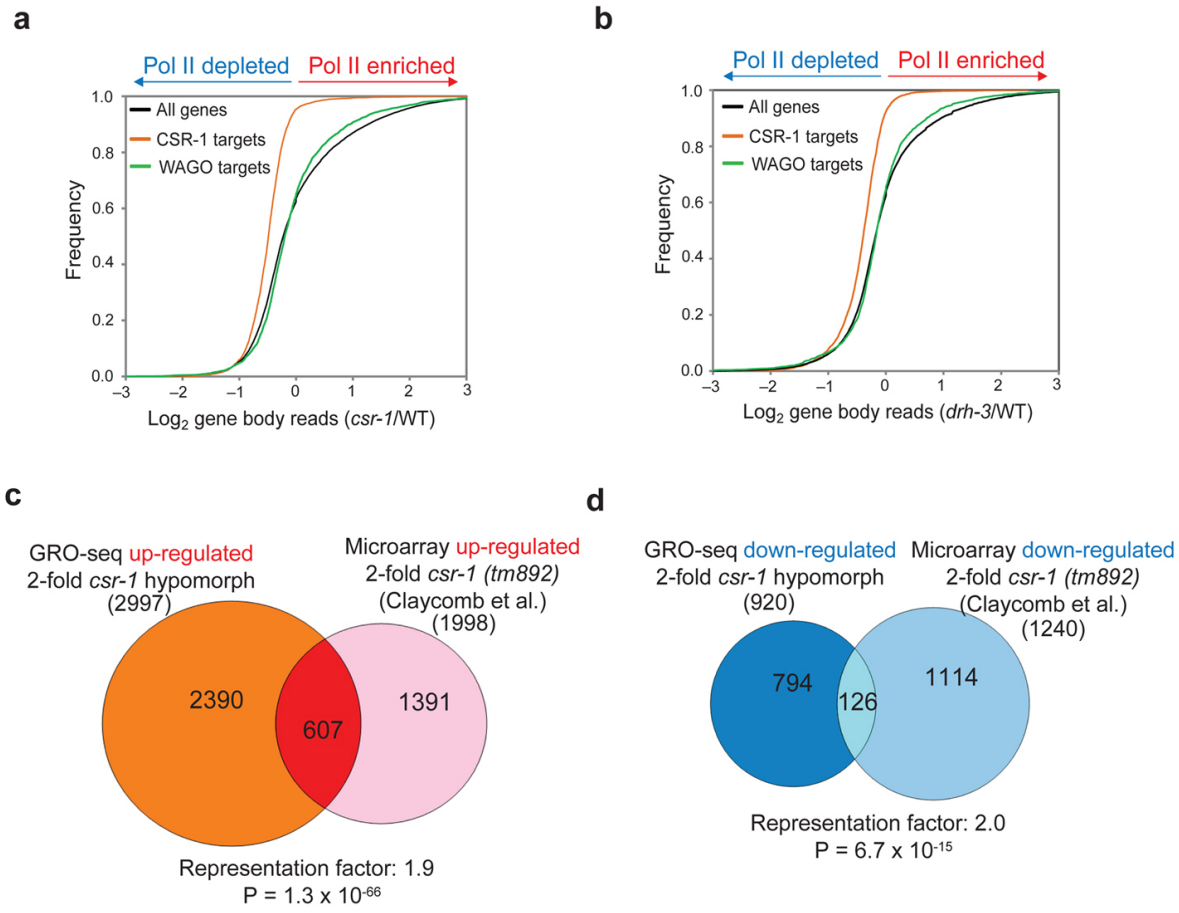

Supplementary Figure 2. Transcription of WAGO target protein-coding genes is not globally affected in *csr-1* hypomorph and *drh-3(ne4253)* mutants; GRO-seq and published microarray data show correlation. (a) Cumulative distribution plots of normalized GRO-seq gene body reads ($\log_2$ of the *csr-1*/WT read ratio) showing the overall effect of *csr-1* mutation on Pol II transcription of CSR-1 targets[15] (orange line), WAGO protein-coding gene targets[14] (purple line) and total genes (black line). (**b)** GRO-seq analysis performed as in **a**, considering *drh-3(ne4253)* and WT normalized GRO-seq gene body reads. **(c)** Venn diagrams showing significant overlaps between the groups of genes found up-regulated in *csr-1* mutant by GRO-seq (this study) and tiling array[15]. A Fisher's exact test was used for calculating *P* values for the significance of the overlaps. **(d)** Venn diagrams as in (c) considering the down-regulated groups of genes identified by both approaches.

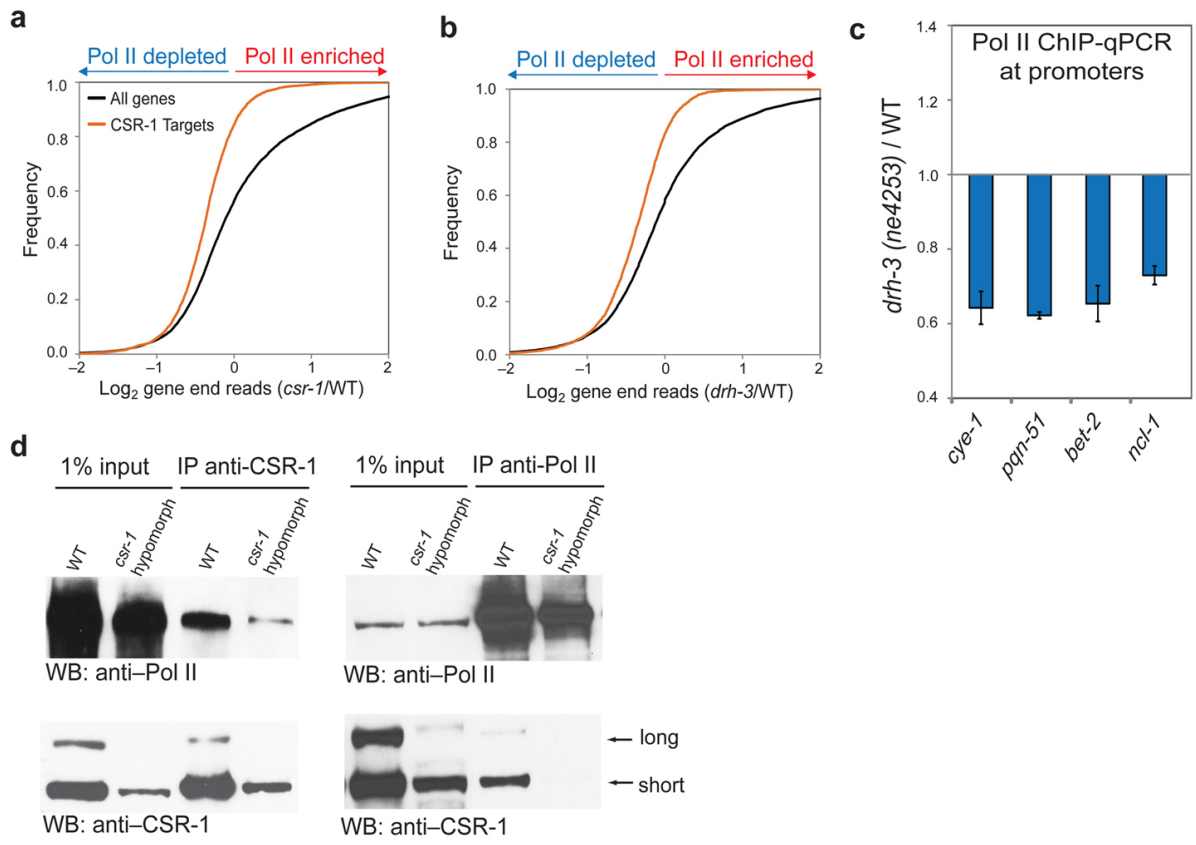

Supplementary Figure 3. CSR-1 affects Pol II transcription at promoters and gene ends and interacts with Pol II. (a, b) Cumulative distribution plots of normalized GRO-seq gene end reads ($\log_2$ of the reads' ratios: *csr-1* hypomorph/WT or *drh-3(ne4253)*/WT) showing the overall effects of *csr-1* or *drh-3* mutations on Pol II transcription at the gene end of CSR-1 targets (orange line), and all genes (black line). **(c)** ChIP-qPCR results in L4 staged worms showing the reduction of Pol II binding at the promoters of CSR-1 target genes in *drh-3(ne4253)* versus WT. Error bars indicate the range (n = 2 nematode cultures). **(d)** Co-immunopercipitation results with nuclear extracts from WT worms and *csr-1* hypomorphic mutant strain show specific interaction between CSR-1 and the Pol II complex. The top panels show western blots with an antibody that recognizes the non-phosphorylated isoform of Pol II and the bottom panels show western blots with an antibody recognizing the long and the short isoforms of CSR-1. Left panels show immunoprecipitation with CSR-1 antibody and right panels show immunoprecipitation with Pol II antibody. Long and short CSR-1 isoforms are indicated by the arrows.

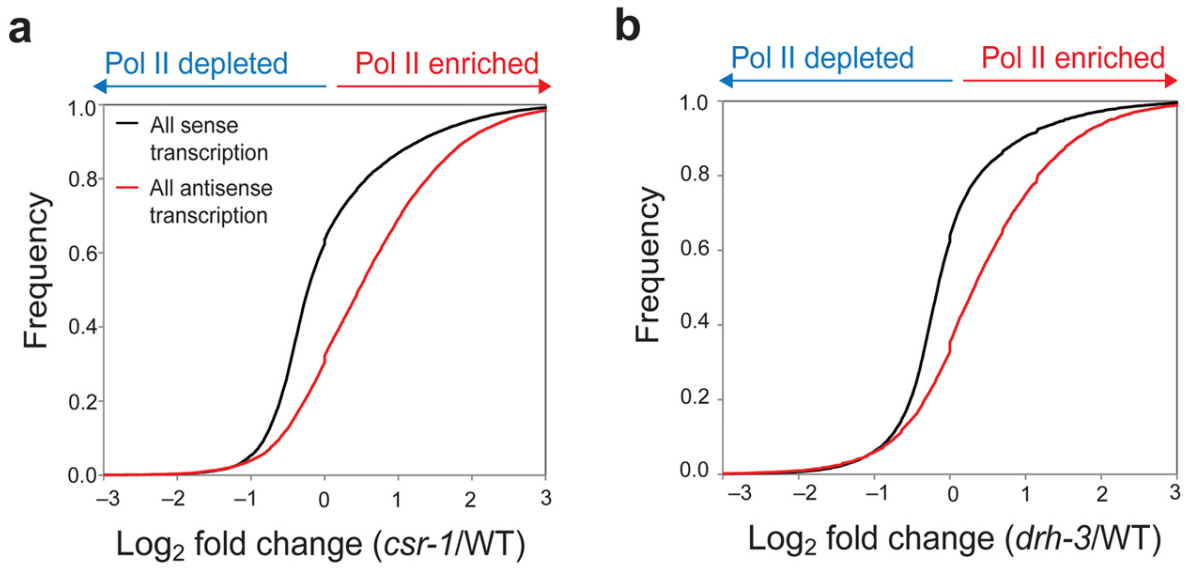

Supplementary Figure 4. Increased antisense Pol II transcription in CSR-1 pathway mutants. (a, b) Cumulative distribution plots of normalized GRO-seq reads showing the global increase in antisense transcription (red line) compared to the sense transcription (black line) in *csr-1* and *drh-3* mutants.

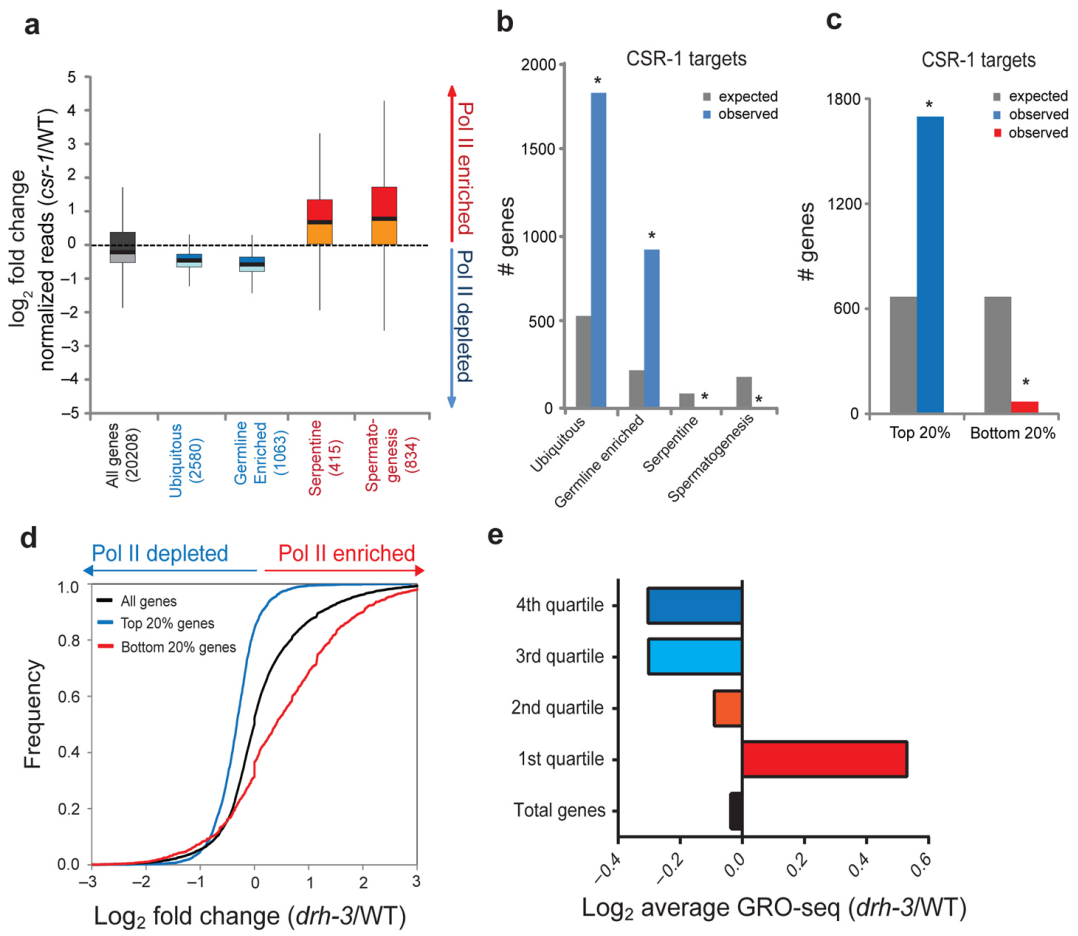

Supplementary Figure 5. Categories of genes affected by CSR-1 pathway mutants. (a) Box plot showing changes in Pol II transcription in *csr-1* mutant versus WT among different categories of genes defined by their expression profiles. The number of genes in each category is shown in parentheses. Each box shows the median (black line), the 25th-75th percentile (box) ± 1.5 interquartile range (whiskers). The boxes in each gene category show significant changes compared to all genes, based on Wilcoxon rank-sum test with *P* value < 0.0001. **(b)** Expected (grey bars) and observed (blue bars) numbers of CSR-1 target genes among different expression categories. Asterisks indicate significance as more or less genes than expected by chance calculated using hypergeometric test, $P < 0.0001$. **(c)** Expected (grey bars) and observed (colored bars) numbers of CSR-1 target genes among the top 20% highly-transcribed genes and the bottom 20%. Asterisks indicate significance as more or less genes than expected by chance calculated using hypergeometric test, $P < 0.0001$. **(d)** Cumulative distribution plots of normalized GRO-seq gene body reads showing the effect of *drh-3(ne4253)* on the top 20% highly-transcribed genes (blue line), the bottom 20% genes (red line) and all genes (black line). Only reads from the gene body were considered for this analysis. **(e)** The average of the $\log_2$ ratios between the *drh-3(ne4253)* mutant and WT normalized gene body reads quantified for genes grouped by quartiles of expression based on GRO-seq.

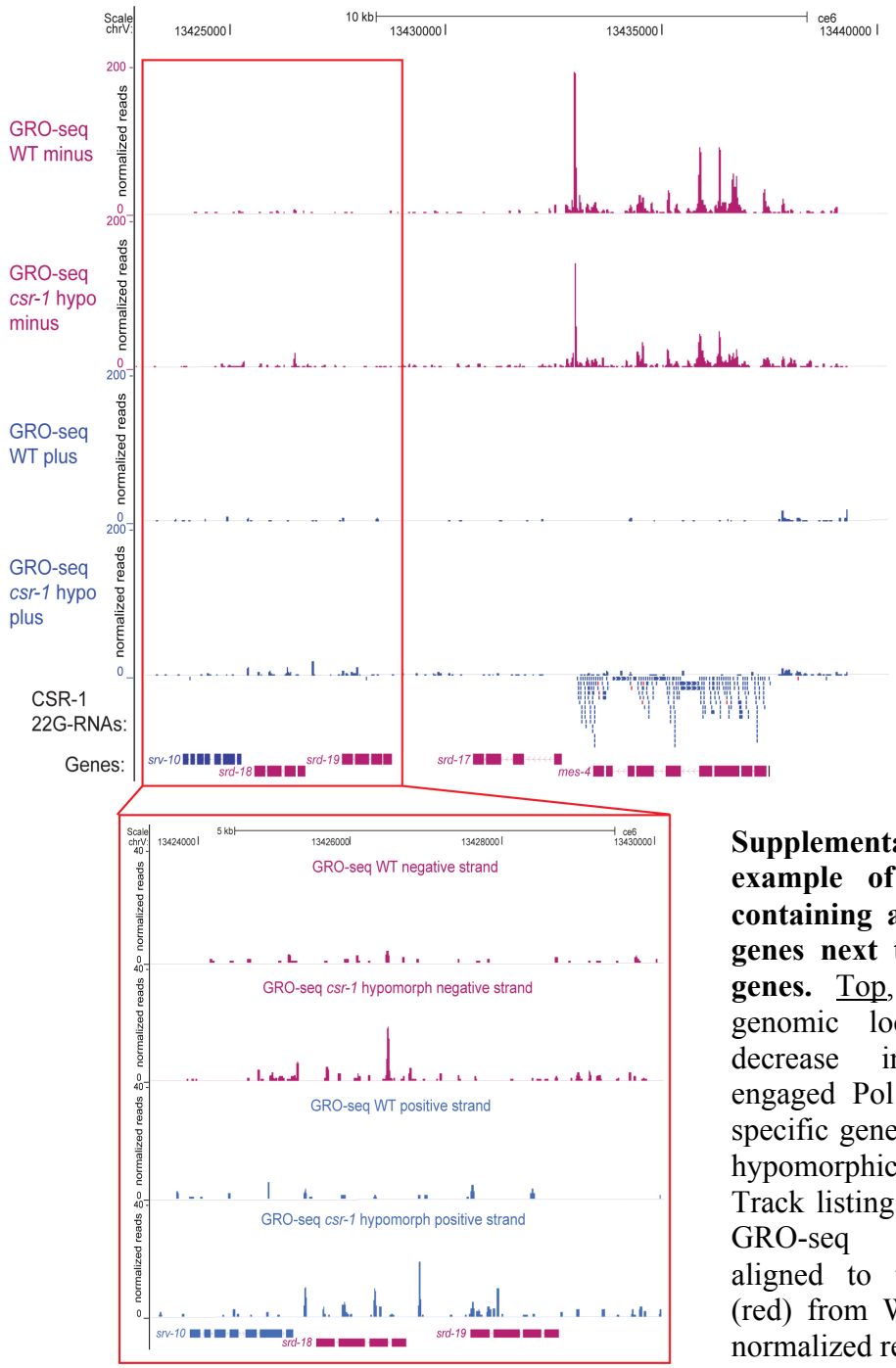

Supplementary Figure 6. An example of a genomic locus containing active CSR-1 target genes next to silent non-target genes. Top, an example of a genomic locus that shows a decrease in transcriptionally-engaged Pol II at the germline-specific gene (*mes-4*) in the *csr-1* hypomorphic mutant versus WT. Track listing from top to bottom: GRO-seq normalized reads aligned to the negative strand (red) from WT larvae, GRO-seq normalized reads aligned to the negative strand (red) from the *csr-1* hypomorphic larvae, GRO-seq normalized reads aligned to the positive strand (blue) from WT larvae (blue), GRO-seq normalized reads aligned to the positive strand (blue) from the *csr-1* hypomorphic larvae. Bottom, a rescaled view of GRO-seq normalized reads to appreciate the increased transcription of non-target silenced genes next to the active CSR-1 target gene in the *csr-1* hypomorphic mutant compared to WT. CSR-1 22G-RNA track shows reads from CSR-1 IP performed on wild type young adult worms and reported in ref. 15. Gene models are based on UCSC Genome Browser (ce06).

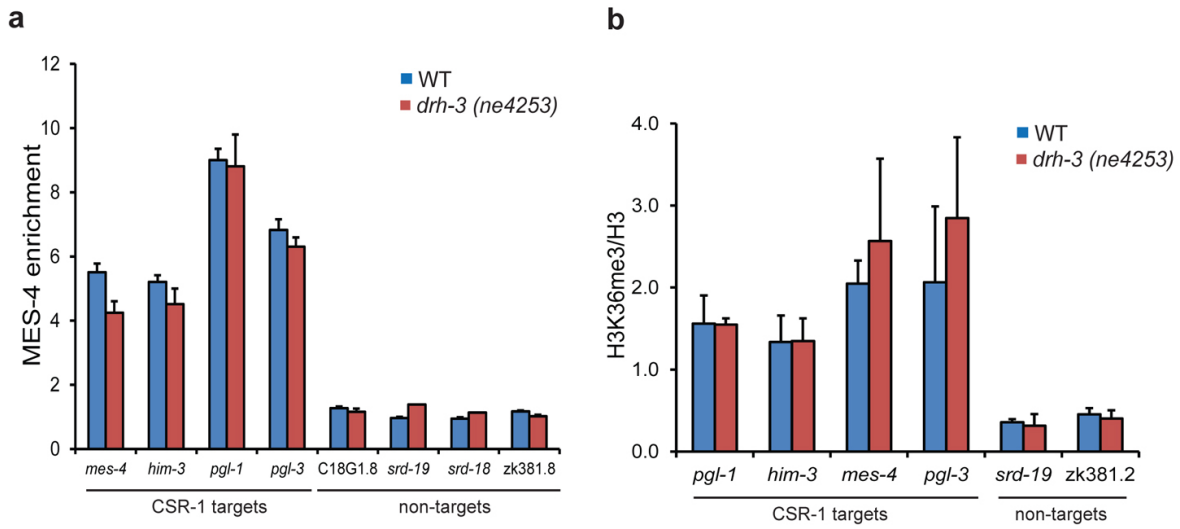

Supplementary Figure 7. CSR-1 regulates transcription independently of MES-4. (a) ChIP-qPCR results with L4 staged worms showing the enrichment of MES-4 at CSR-1 target regions compared to the non-target regions. There are no differences in MES-4 binding in *drh-3(ne4253)* mutant compared to WT. The enrichment has been calculated relative to the non-target gene ZK381.2. Error bars indicate the range (n = 2 nematode cultures). **(b)** ChIP-qPCR results with L4-staged worms, as in (a), showing the levels of H3K36me3 normalized to the total levels of histone H3 at CSR-1 target regions compared to the non-target regions. There are no differences in the levels of H3K36me3 in *drh-3(ne4253)* mutant compared to WT. Error bars indicate the range (n = 2 nematode cultures).

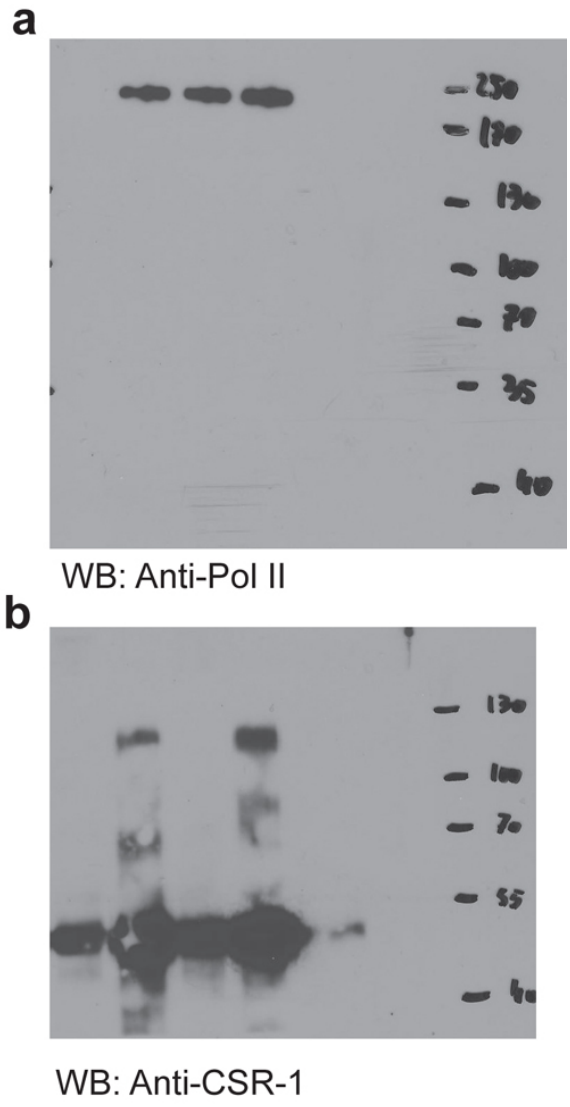

Supplementary Figure 8. Uncropped images of blots shown in Figure 2c: (a) related to Figure 2c (top), (b) related to Figure 2c (bottom).